Supporting Information

[Cu(4-phenylpyridine)$_4$(trifluoromethanesulfonate)$_2$], a Werner complex that exhibits high selectivity for *o*-xylene

*Adrianna M. Kałuża, Soumya Mukherjee, Shi-Qiang Wang, Daniel J. O'Hearn and Michael J. Zaworotko**

**E-mail: xtal@ul.ie*

Table of Contents

1. Experimental section

All materials were used as received from commercial sources.

Synthesis of closed (α–) phase

SAMM-3-Cu-OTf was synthesised by mixing an ethanolic solution of 4-phenylpyridine with an ethanolic solution of copper trifluoromethanesulfonate in a 4:1 molar ratio. The solution was stirred at room temperature (rt) for *ca.* 2 hours, resulting in the formation of a dark blue precipitate. 3 mL of distilled water was added in order to facilitate full precipitation of the complex out of solution. The precipitate was then filtered, washed with distilled water and dried in the oven at 85 °C to obtain the α–phase. This was followed by the formation of a dark blue crystalline powder, which was obtained with 100% atom economy and ~ 85% yield. Single crystals were isolated by recrystallising the powder from ethanol by slow evaporation or by layering with hexane. This afforded dark blue, block-shaped crystals of the α–phase.

Synthesis of phase I

Single crystals of **SAMM-3-Cu-OTf·4OX** were prepared by placing *ca*. 12 mg of the α–phase in 3 mL of OX and stirring at 50 °C overnight, turning the solution bright green. On standing at rt over ~3 days, purple, block-shaped crystals suitable for single crystal X-ray diffraction studies were isolated.

Synthesis of phase II

Phase **II** was prepared by placing *ca.* 12 mg of the α–phase in 3 mL of an equimolar binary isomer mixture containing OX, *i.e.* OX/MX, OX/PX or OX/EB. It was then stirred at 50 °C overnight, turning the solution a light blue colour. After standing at rt over 2-3 days, some purple, block-shaped crystals suitable for single crystal X-ray diffraction studies were isolated.

2. CO_2 gas sorption

Gas sorption measurements were carried out between 0 – 1 bar on a Micromeritics TriStar II PLUS (195 K CO_2). **SAMM-3-Cu-OTf** was degassed at 70 °C for 2 hours on a SmartVacPrep™ degassing station. Temperature on the Tristar II Plus porosimeter was controlled with a dry ice-acetone mixture in a 4 L dewar flask (195 K).

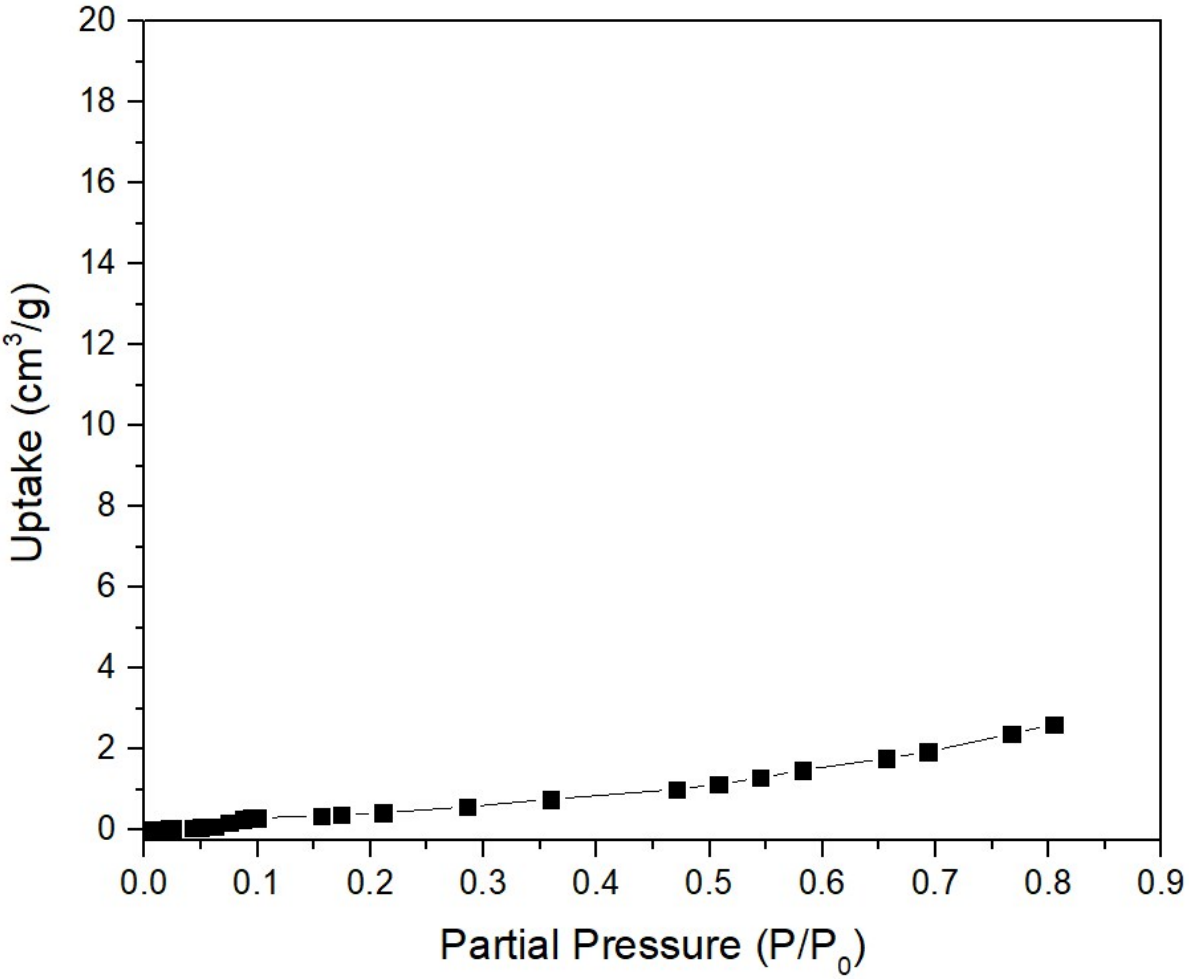

Figure S1: CO_2 adsorption isotherm at 195K recorded for **SAMM-3-Cu-OTf**.

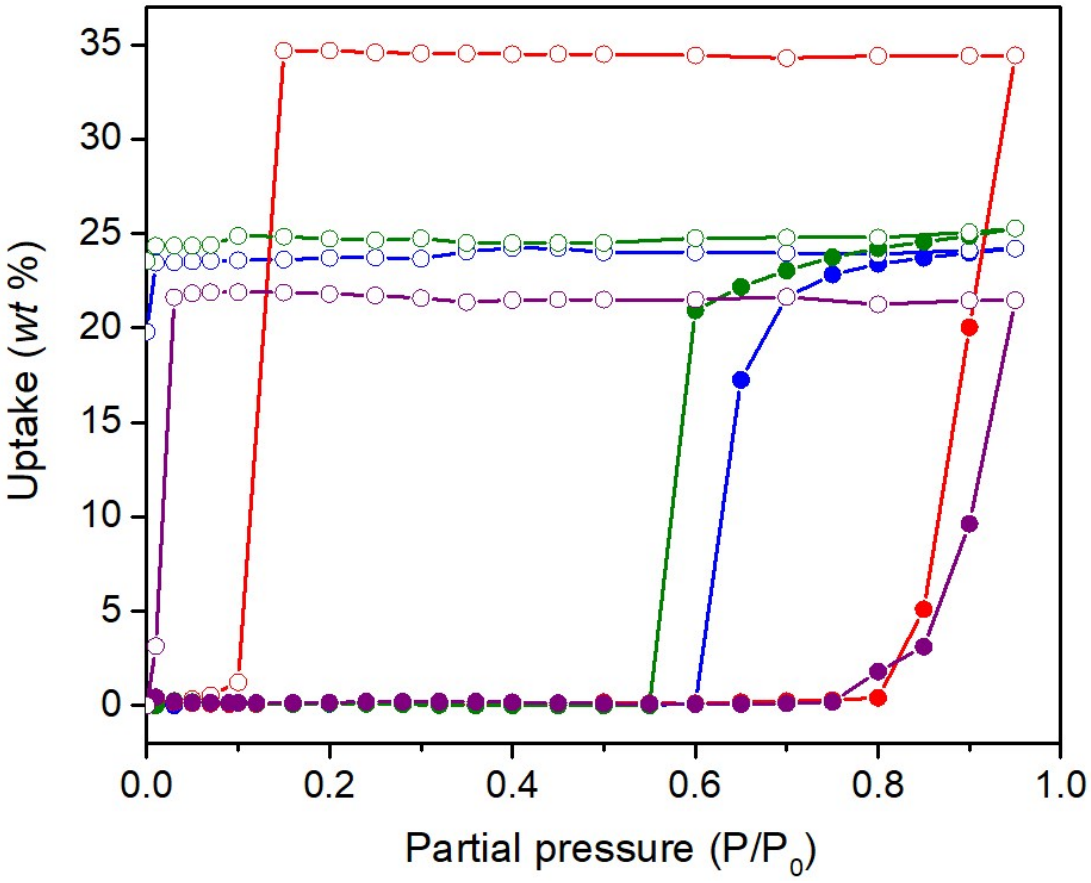

Figure S2: Sorption isotherms of OX (green), MX (blue), PX (red) and EB (purple) on **SAMM-3-Ni-NCS**. Filled symbols represent adsorption and blank symbols represent desorption.

3. Powder X-ray Diffraction (PXRD)

PXRD experiments were conducted using microcrystalline powder samples on a Panalytical Empyrean diffractometer (40 kV, 40 mA) using Cu Kα radiation (λ = 1.5418 Å) in Bragg-Brentano geometry. A scan speed of 0.111747°/s (6.7°/min), with a step size of 0.026° in 2θ was used at room temperature with a range of 5° < 2θ < 40°.

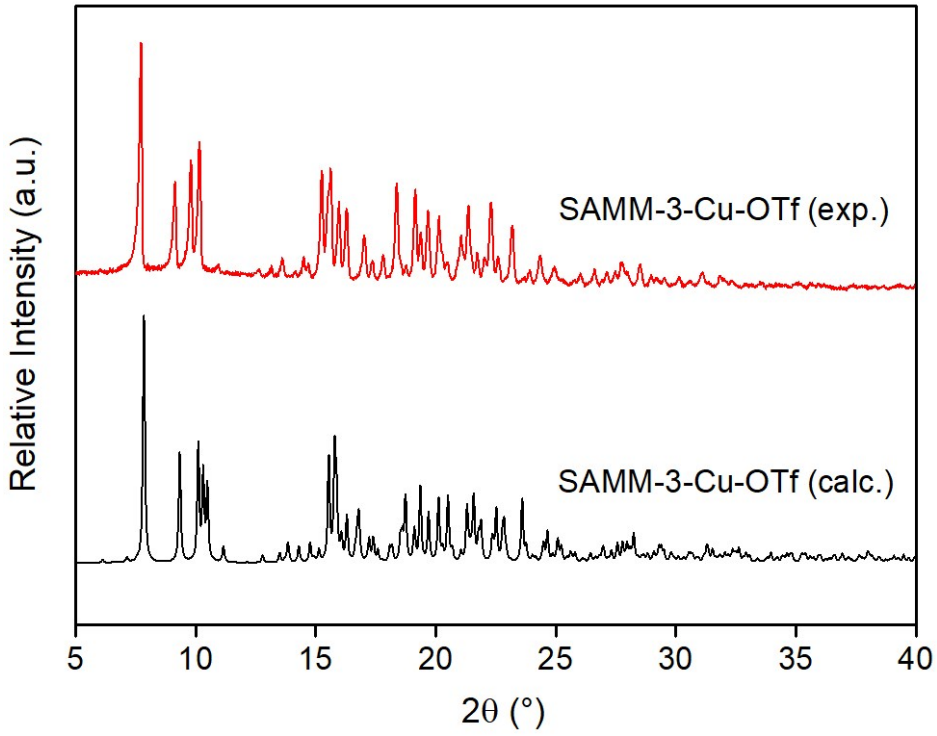

Figure S3: Bottom: Calculated (calc.) PXRD from the single crystal structure of **SAMM-3-Cu-OTf**. Top: PXRD of the bulk powder of **SAMM-3-Cu-OTf**, obtained experimentally (exp.).

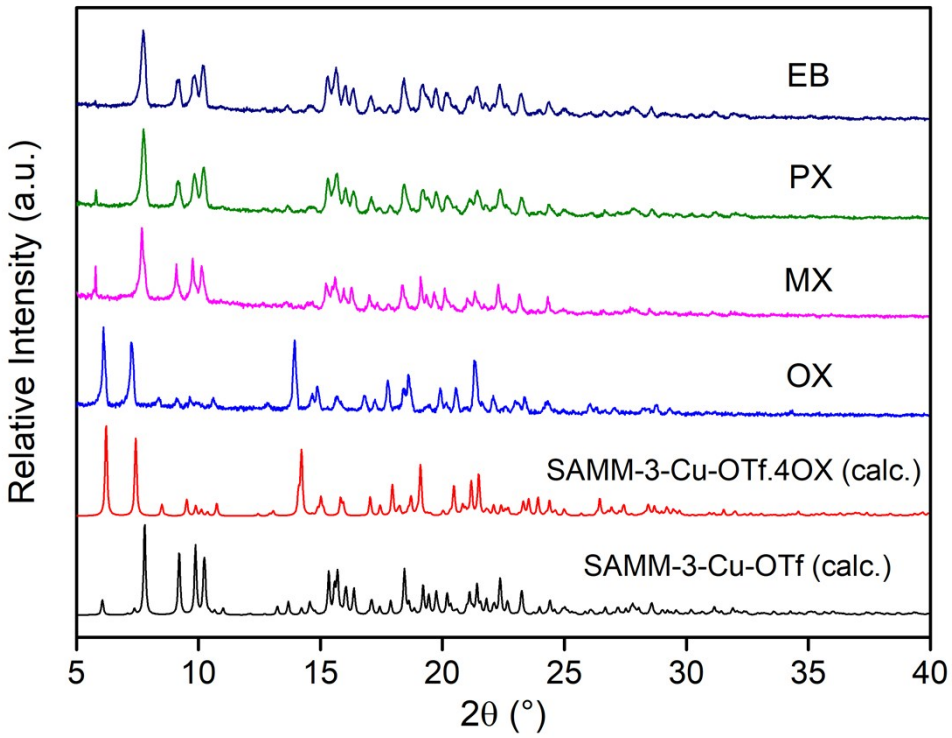

Figure S4: From bottom to top: Calculated (calc.) powder pattern of the closed phase **SAMM-3-Cu-OTf**; calc. powder pattern of the open phase **SAMM-3-Cu-OTf.4OX**; experimental patterns obtained by soaking the non-porous **SAMM-3-Cu-OTf** for 18 h in OX, MX, PX and EB respectively.

4. Thermogravimetric Analysis (TGA)

Thermogravimetric studies were carried out under a steady flow of N_2 (balance purge flow rate = 40 mL/min, sample purge flow rate = 60 mL/min) in a "TA Instruments" Q50 thermal analyser. The heating rate was kept constant at 10 ºC/min.

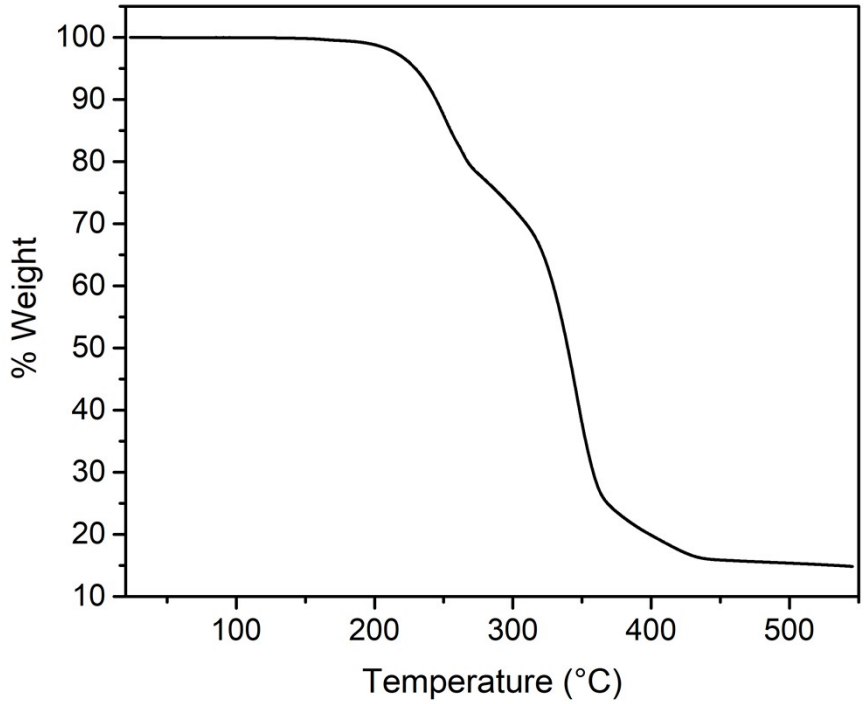

Figure S5: Thermogravimetric analysis (TGA) pattern of **SAMM-3-Cu-OTf**.

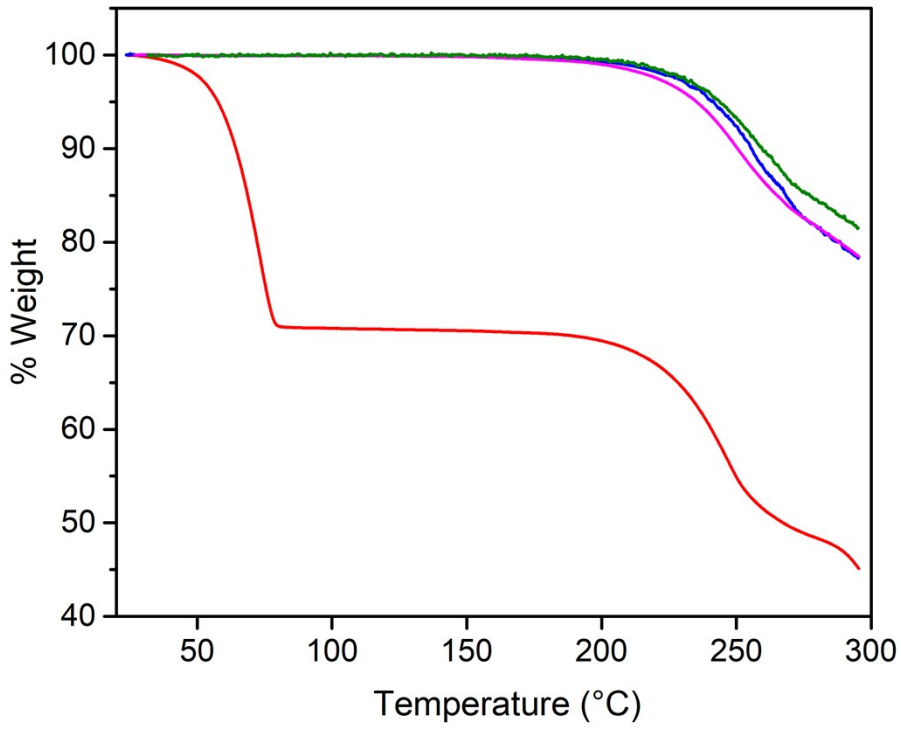

Figure S6: TGA patterns of dried samples of **SAMM-3-Cu-OTf** which were soaked for 18 h in OX (red), MX (blue), PX (pink) and EB (green).

5. Vacuum Dynamic Vapour Sorption

Dynamic vapour sorption measurements were conducted using a Surface Measurement Systems DVS Vacuum at 298 K. Samples of **SAMM-3-Cu-OTf** were further degassed under high vacuum ($1x10^{-5}$ Torr) *in-situ* and stepwise increase in relative pressure from 0 to 95% were controlled by equilibrated weight changes of the sample (dM/dT = 0.01%/min). The minimum and maximum equilibration time for each step were 10 and 600 min, respectively. Vacuum pressure transducers were used with ability to measure from $1x10^{-6}$ to 760 Torr with a resolution of 0.01%. Approximately 10 mg of sample was used for each experiment. The mass of the sample was determined by comparison to an empty reference pan and recorded by a high resolution microbalance with a precision of 0.1 μg. In order to study the kinetics of OX sorption on **SAMM-3-Cu-OTf**, the powder sample was first degassed for half hour and then exposed to 95% relative pressure of OX for 24 hours. For OX adsorption-desorption recyclability test, **SAMM-3-Cu-OTf** was first degassed for half hour. Then the sample was exposed to 95% relative pressure of OX for 20 hours as the adsorption step; and exposed to vacuum for 2 hours as the desorption step.

6. Scanning Electron Microscopy (SEM)

SEM images were collected using SU 70 Hitachi instrument (10 kV, 28 μA). The images were collected on two separate batches: one prior to vacuum DVS measurements and one after five sorption cycles of OX. The samples were sputter-coated with gold (20 mA, 60 s) prior to imaging.

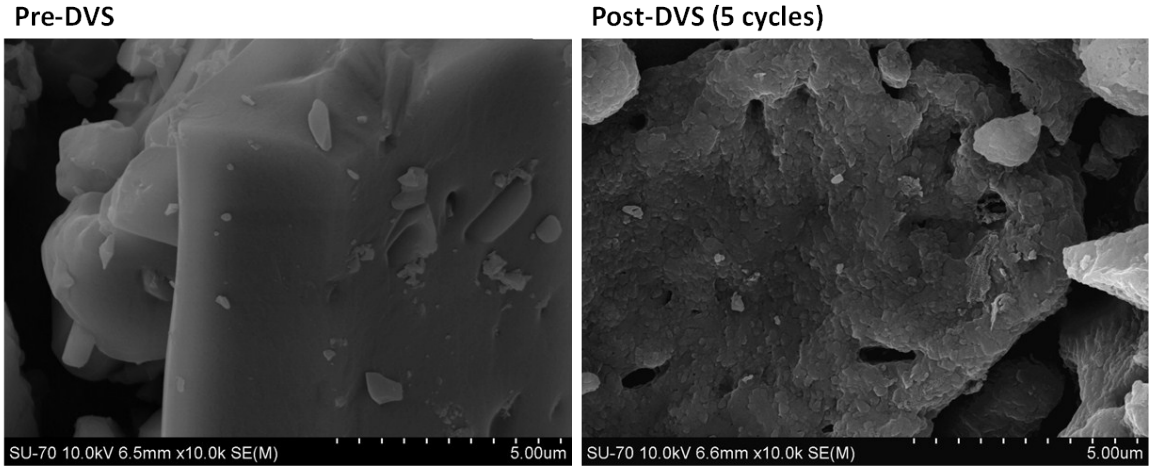

Figure S7: Comparison of **SAMM-3-Cu-OTf** particle surface before DVS measurement (left) and after five DVS OX cycles (right).

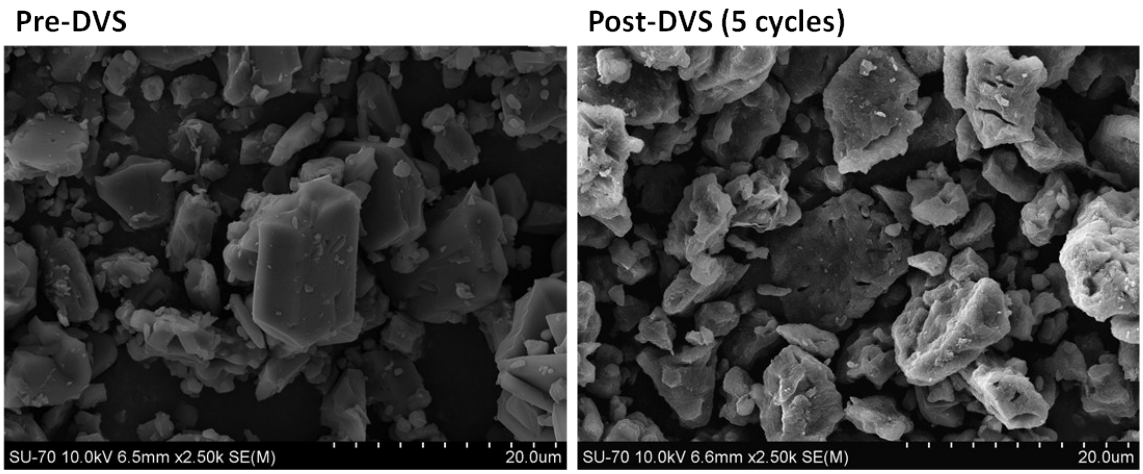

Figure S8: SEM of **SAMM-3-Cu-OTf** in the 20 μm range, showing possible reduction in adhesiveness of the particles after 5 OX cycles by DVS.

7. Single Crystal X-ray Crystallography

Suitable single crystals of all compounds were chosen for single crystal X-ray diffraction measurements. The data was collected on a Bruker D8 Quest diffractometer equipped with MoKα source (λ = 0.71073 Å) and Photon 100 detector. For low temperature measurements, a nitrogen flow from Oxford Cryosystems was used. In all cases, data was indexed, integrated and scaled in APEX3.[S1] Absorption correction was performed by multi-scan method using SADABS.[S2] Space group determinations were performed with the assistance of XPREP[S3] as implemented in APEX3. Structure solutions were obtained using the intrinsic phasing method (SHELXT)[S4] and refined on F^2 using SHELXL[S5] non-linear least squares as implemented in OLEX^2 v1.2.10.[S6] All non-hydrogen atoms were refined anisotropically (with the exception of some disorders; details for each disorder are given below). Hydrogen atoms were added at calculated positions and refined using the riding model. All difference maps were calculated using Olex^2. Crystallographic data for all compounds are summarised in the Crystallographic Tables section. All disorders were treated by refining the appropriate occupancies using additional free variable(s) and appropriate constraints, and by placing the disordered atoms in the appropriate parts. All crystal structures have been deposited in the Cambridge Crystallographic Data Centre (CCDC 1953546-1953550).

(a) SAMM-3-Cu-OTf@OX/PX

One of the pyridyl rings of one of the 4-phenylpyridine ligands was disordered by rotation about the axis running the length of the ligand. The ring was found to occupy two positions, for which the occupancies were refined using a free variable (FVAR #2 = 0.541(8)). One

of the two OX molecules was found to be positionally disordered. This was modelled as two OX molecules (FVAR #3 = 0.518(11)), however, as shown in the difference map in Figure S9, there is still significant electron density that has not been accounted for. The electron density about this position was too diffuse to model further, and thus the two positions were refined isotropically with the appropriate AFIX66 commands.

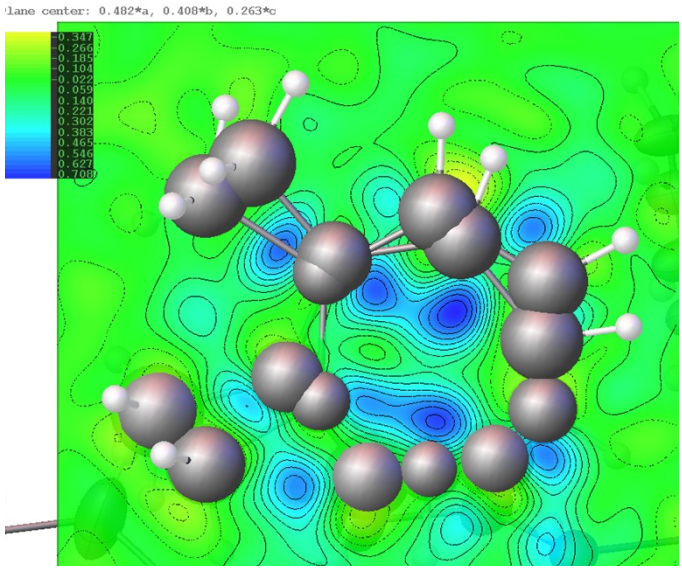

Figure S9: Difference map for the positionally disordered OX molecule in **SAMM-3-Cu-OTf@OX/PX**. FVAR #3 = 0.518(11).

(b) SAMM-3-Cu-OTf@OX/MX

One of the pyridyl rings of one of the 4-phenylpyridine ligands was disordered by rotation about the axis running the length of the ligand. The ring was found to occupy two positions, for which the occupancies were refined using a free variable (FVAR #2 = 0.524(7)). One of the two OX molecules was found to be positionally disordered. This was modelled as two OX molecules, however, as shown in the difference map in Figure S10, there is still significant electron density that has not been accounted for. The electron density about this position was too diffuse to model further, and thus the two rings were refined isotropically with the appropriate AFIX66 commands (FVAR #3 = 0.544(9)). The other xylene site was found to be a substitutionally disordered between an OX molecule (occupancy = 0.733(8)) and a MX molecule (occupancy =0.267(8)) (FVAR #4 = 0.733(8)). Both molecules could be refined anisotropically with the appropriate AFIX66 commands, and no significant residual electron density was found by the difference map (Figure S11).

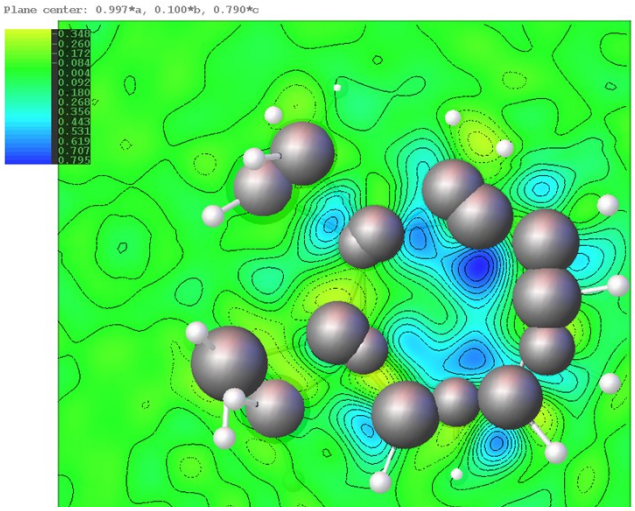

Figure S10: Difference map for the positionally disordered OX molecule in **SAMM-3-Cu-OTf@OX/MX**. FVAR #3 = 0.543(9).

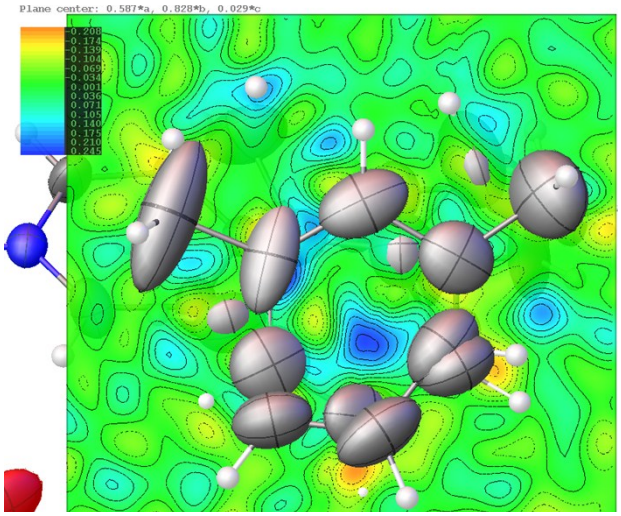

Figure S11: Difference map for the substitutionally disordered site in **SAMM-3-Cu-OTf@OX/MX**. FVAR #4 = 0.733(8).

(c) SAMM-3-Cu-OTf@OX/EB

One of the pyridyl rings of one of the 4-phenylpyridine ligands was disordered by rotation about the axis running the length of the ligand. The ring was found to occupy two positions, for which the occupancies were refined using a free variable (FVAR #2 = 0.446(8)). One of the two OX molecules were found to be positionally disordered. This was modelled as two OX molecules, however, as shown in the difference map in Figure S12, there is still significant electron density that has not been accounted for. The electron density about this position was too diffuse to model further, and thus the two rings were refined isotropically

with the appropriate AFIX66 commands (FVAR #3 = 0.536(11)). The other OX site was treated in a similar way (FVAR #4 = 0.623(18)) (difference map Figure S13).

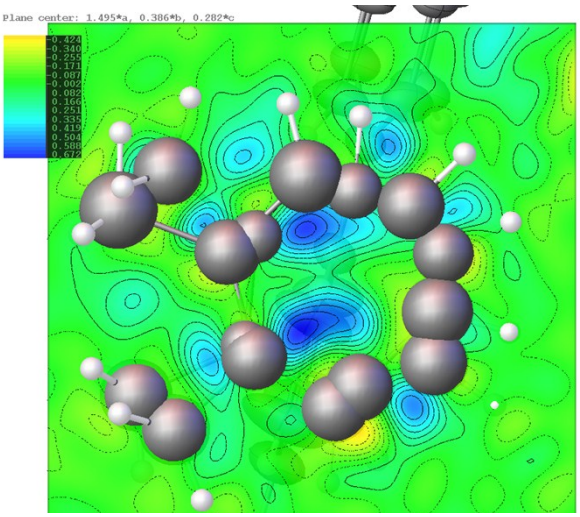

Figure S12: Difference map for one of the positionally disordered sites in **SAMM-3-Cu-OTf@OX/EB.** FVAR #3 = 0.536(11).

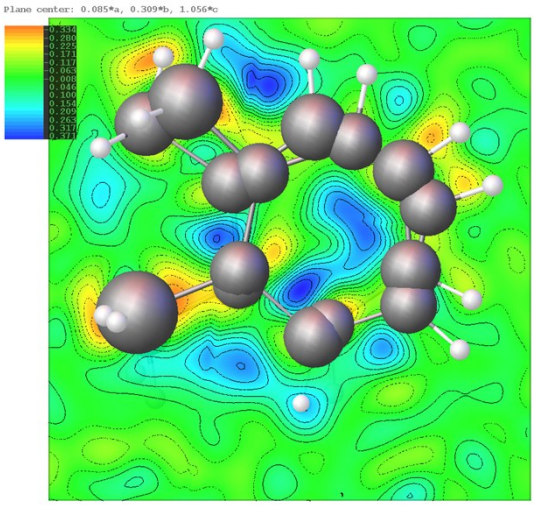

Figure S13: Difference map for one of the positionally disordered sites in **SAMM-3-Cu-OTf@OX/EB.** FVAR #4 = 0.623(18).

8. Crystallographic Tables

SAMM-3-Cu-OTf_alpha

Identification code	SAMM-3-Cu-OTf_alpha
Empirical formula	$C_{46}H_{36}CuF_6N_4O_6S_2$
Formula weight	982.45
Temperature/K	150.0
Crystal system	triclinic
Space group	P*1*
a/Å	11.743(3)
b/Å	13.021(4)
c/Å	15.225(4)
α/°	72.071(10)
β/°	85.436(10)
γ/°	89.509(12)
Volume/Å^3	2207.6(10)
Z	2
ρ_{calc}g/cm^3	1.478
μ/mm^{-1}	0.668
F(000)	1006.0
Crystal size/mm^3	0.45 × 0.45 × 0.38
Radiation	MoKα (λ = 0.71076)
2θ range for data collection/°	4.95 to 59.204
Index ranges	$-16 \leq h \leq 16$, $-18 \leq k \leq 18$, $-21 \leq l \leq 21$
Reflections collected	53982
Independent reflections	24095 [R_{int} = 0.0409, R_{sigma} = 0.0667]
Data/restraints/parameters	24095/3/1173
Goodness-of-fit on F^2	1.042
Final R indexes [I>=2σ (I)]	R_1 = 0.0636, wR_2 = 0.1659
Final R indexes [all data]	R_1 = 0.0745, wR_2 = 0.1720
Largest diff. peak/hole / e Å^{-3}	1.99/-0.74
Flack parameter	0.077(14)

SAMM-3-Cu-OTf@OX

Identification code	SAMM-3-Cu-OTf@OX
Empirical formula	$C_{78}H_{76}CuF_6N_4O_6S_2$
Formula weight	1407.08
Temperature/K	155
Crystal system	triclinic
Space group	*P-1*
a/Å	10.1269(3)
b/Å	13.1476(2)
c/Å	29.1917(6)
α/°	97.3190(10)
β/°	96.976(2)
γ/°	111.490(2)
Volume/Å^3	3527.03(15)
Z	2
ρ_{calc}g/cm^3	1.325
μ/mm^{-1}	1.586
F(000)	1470.0
Crystal size/mm^3	0.32 × 0.23 × 0.16
Radiation	CuKα (λ = 1.54184)
2θ range for data collection/°	7.354 to 133.404
Index ranges	$-12 \leq h \leq 12$, $-15 \leq k \leq 15$, $-34 \leq l \leq 34$
Reflections collected	44664
Independent reflections	12127 [R_{int} = 0.0397, R_{sigma} = 0.0390]
Data/restraints/parameters	12127/0/899
Goodness-of-fit on F^2	1.067
Final R indexes [I>=2σ (I)]	R_1 = 0.0609, wR_2 = 0.1666
Final R indexes [all data]	R_1 = 0.0690, wR_2 = 0.1883
Largest diff. peak/hole / e Å^{-3}	0.84/-0.77

SAMM-3-Cu-OTf@OX/MX

Identification code	SAMM-3-Cu-OTf@OX_MX
Empirical formula	$C_{78}H_{76}CuF_6N_4O_6S_2$
Formula weight	1407.08
Temperature/K	150
Crystal system	triclinic
Space group	*P-1*
a/Å	10.166(2)
b/Å	13.051(3)
c/Å	15.236(4)
α/°	72.382(7)
β/°	74.260(7)
γ/°	69.168(6)
Volume/Å^3	1769.9(7)
Z	1
ρ_{calc}g/cm^3	1.320
μ/mm^{-1}	0.439
F(000)	735.0
Crystal size/mm^3	0.41 × 0.35 × 0.31
Radiation	MoKα (λ = 0.71076)
2θ range for data collection/°	5.634 to 57.39
Index ranges	$-13 \leq h \leq 13$, $-17 \leq k \leq 17$, $-20 \leq l \leq 20$
Reflections collected	37311
Independent reflections	9116 [R_{int} = 0.0236, R_{sigma} = 0.0221]
Data/restraints/parameters	9116/0/502
Goodness-of-fit on F^2	1.035
Final R indexes [I>=2σ (I)]	R_1 = 0.0617, wR_2 = 0.1599
Final R indexes [all data]	R_1 = 0.0747, wR_2 = 0.1708
Largest diff. peak/hole / e Å^{-3}	1.19/-1.12

SAMM-3-Cu-OTf@OX/PX

Identification code	SAMM-3-Cu-OTf@OX_PX
Empirical formula	$C_{78}H_{76}CuF_6N_4O_6S_2$
Formula weight	1407.08
Temperature/K	150.0
Crystal system	triclinic
Space group	*P-1*
a/Å	10.2443(13)
b/Å	13.0741(16)
c/Å	15.129(2)
α/°	72.449(5)
β/°	73.851(5)
γ/°	69.024(4)
Volume/Å^3	1770.7(4)
Z	1
ρ_{calc}g/cm^3	1.320
μ/mm^{-1}	0.439
F(000)	735.0
Crystal size/mm^3	0.39 × 0.31 × 0.29
Radiation	MoKα (λ = 0.71076)
2θ range for data collection/°	5.646 to 57.458
Index ranges	$-13 \leq h \leq 13$, $-17 \leq k \leq 17$, $-20 \leq l \leq 20$
Reflections collected	34123
Independent reflections	9084 [R_{int} = 0.0263, R_{sigma} = 0.0265]
Data/restraints/parameters	9084/0/451
Goodness-of-fit on F^2	1.023
Final R indexes [I>=2σ (I)]	R_1 = 0.0653, wR_2 = 0.1670
Final R indexes [all data]	R_1 = 0.0778, wR_2 = 0.1776
Largest diff. peak/hole / e Å^{-3}	0.90/-1.05

SAMM-3-Cu-OTf@OX/EB

Identification code	SAMM-3-Cu-OTf@OX_EB
Empirical formula	$C_{78}H_{76}CuF_6N_4O_6S_2$
Formula weight	1407.08
Temperature/K	150.0
Crystal system	triclinic
Space group	*P-1*
a/Å	10.249(4)
b/Å	13.097(3)
c/Å	15.188(4)
α/°	72.156(11)
β/°	73.950(16)
γ/°	68.985(15)
Volume/Å^3	1779.5(10)
Z	1
ρ_{calc}g/cm^3	1.313
μ/mm^{-1}	0.437
F(000)	735.0
Crystal size/mm^3	0.41 × 0.32 × 0.28
Radiation	MoKα (λ = 0.71076)
2θ range for data collection/°	5.63 to 57.338
Index ranges	$-13 \leq h \leq 13$, $-17 \leq k \leq 17$, $-20 \leq l \leq 20$
Reflections collected	34925
Independent reflections	9013 [R_{int} = 0.0305, R_{sigma} = 0.0294]
Data/restraints/parameters	9013/0/422
Goodness-of-fit on F^2	1.033
Final R indexes [I>=2σ (I)]	R_1 = 0.0688, wR_2 = 0.1793
Final R indexes [all data]	R_1 = 0.0810, wR_2 = 0.1902
Largest diff. peak/hole / e Å^{-3}	0.91/-1.03

9. ^{1}H NMR studies

(a) Vapour-phase selectivity

Vapour-phase selectivity experiments were performed by placing 20 mg of the crystalline powder of **SAMM-3-Cu-OTf** in a smaller vial and sealing it inside a larger vial containing 30 mL of an equimolar binary mixture of any of the C_8 isomer pairs. After standing for 4 d at rt, the smaller vials were removed and placed in the fume hood for 30 min to eliminate any surface condensation. In each of the binary vapour-phase xylene selectivity experiments, this post-exposure crystalline powder was dissolved in 1.5 mL of deuterated chloroform ($CDCl_3$) to serve as the probe solution for ^{1}H NMR studies. The selectivity values were then determined by considering the average values obtained from three separate experiments performed under identical conditions. Values for MX/PX, MX/EB and PX/EB were omitted, as there were no intensity peaks corresponding to these isomers on the NMR spectrum when OX was not present.

Batch no.	OX/MX	OX/PX	OX/EB
1	6.12	23.13	17.97
2	6.00	22.93	17.90
3	6.11	23.09	18.11
Average	6.08	23.05	17.99

Table S1: Selectivity values for OX-containing isomer mixtures in the vapour phase.

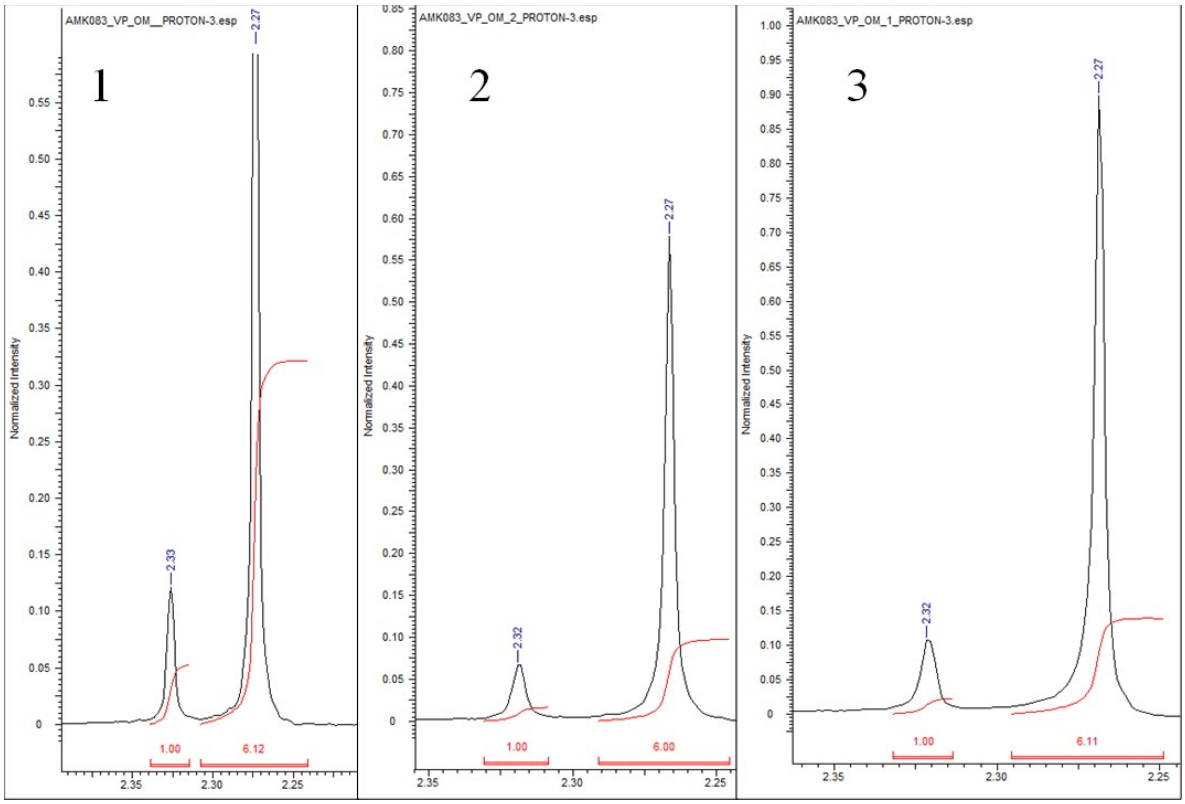

Figure S14: Magnified ^{1}H NMR spectrum for the methyl groups of MX (chemical shift, δ = 2.33/2.32) and OX (δ = 2.27) in **SAMM-3-Cu-OTf**, post equimolar OX/MX vapour exposure.

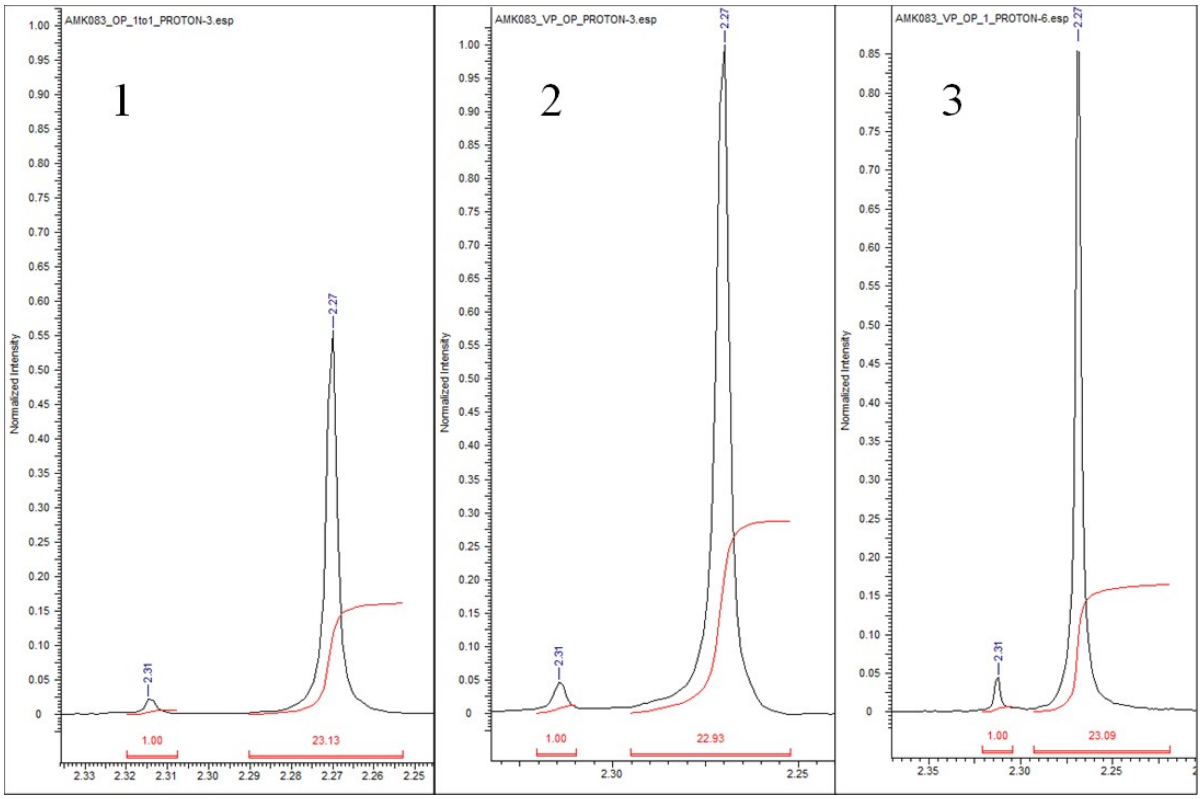

Figure S15: Magnified ^{1}H NMR spectrum for the methyl groups of PX (δ = 2.31) and OX (δ = 2.27) in **SAMM-3-Cu-OTf**, post equimolar OX/PX vapour exposure.

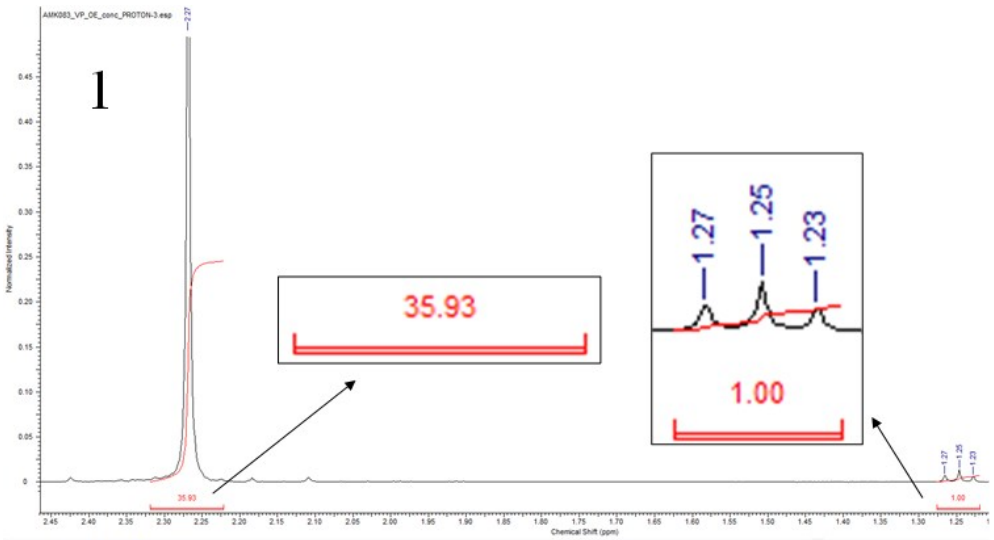
1
35.93
1.27
1.25
1.23
1.00
Chemical Shift (ppm)

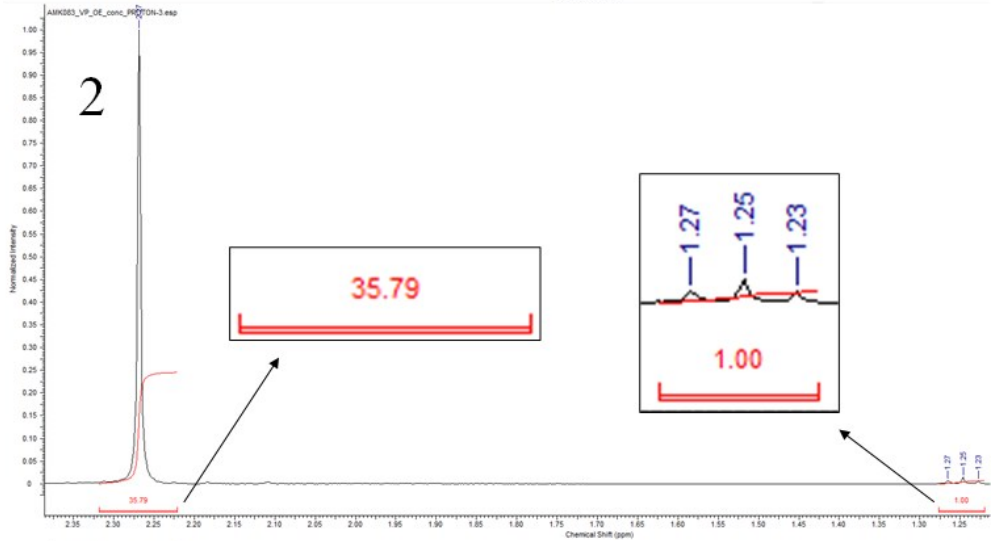
2
35.79
1.27
1.25
1.23
1.00
Chemical Shift (ppm)

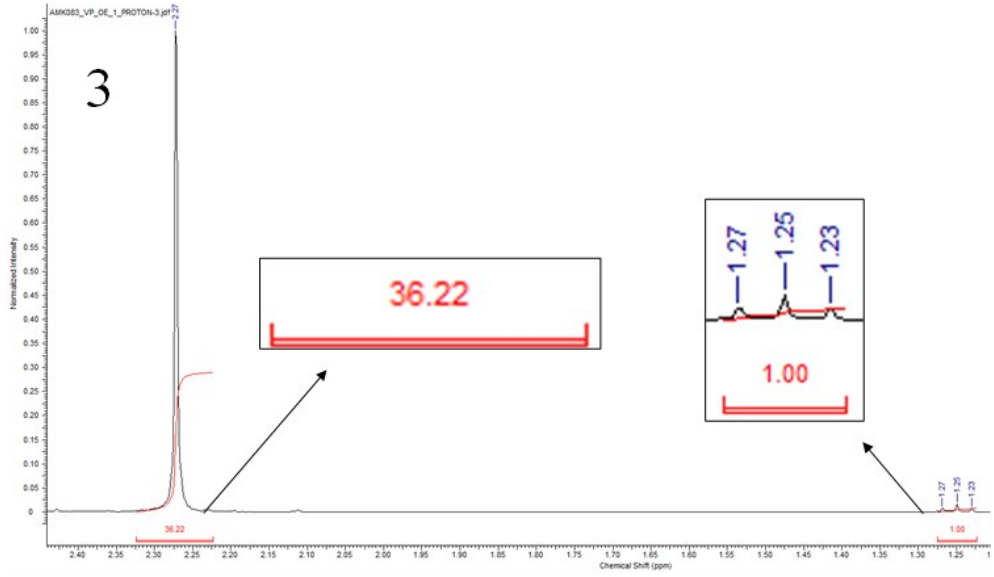
3
36.22
1.27
1.25
1.23
1.00
Chemical Shift (ppm)

Figure S16: Magnified ^{1}H NMR spectrum for the methyl groups of EB (triplet) and OX (singlet) in **SAMM-3-Cu-OTf**, post exposure to an equimolar OX/EB vapour. The methyl group signal for OX represents twice as many protons as EB.

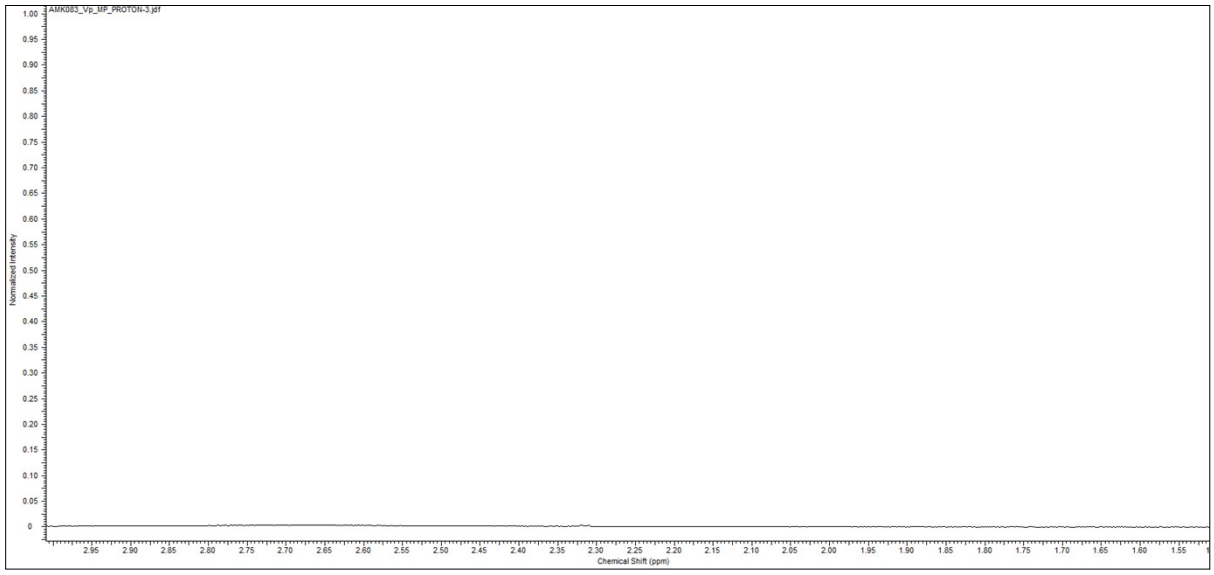

Figure S17: ^{1}H NMR spectrum of **SAMM-3-Cu-OTf**, post-exposure to MX/PX vapour. Magnified region: 1.5 – 3.0 ppm.

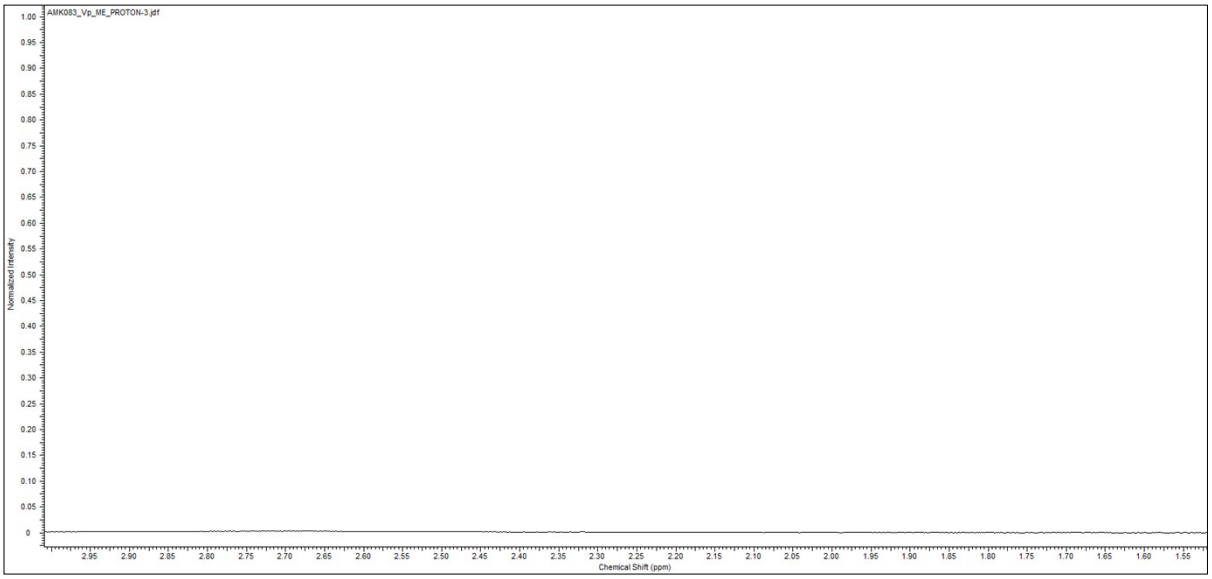

Figure S18: ^{1}H NMR spectrum of **SAMM-3-Cu-OTf**, post-exposure to MX/EB vapour. Magnified region: 1.5 – 3.0 ppm.

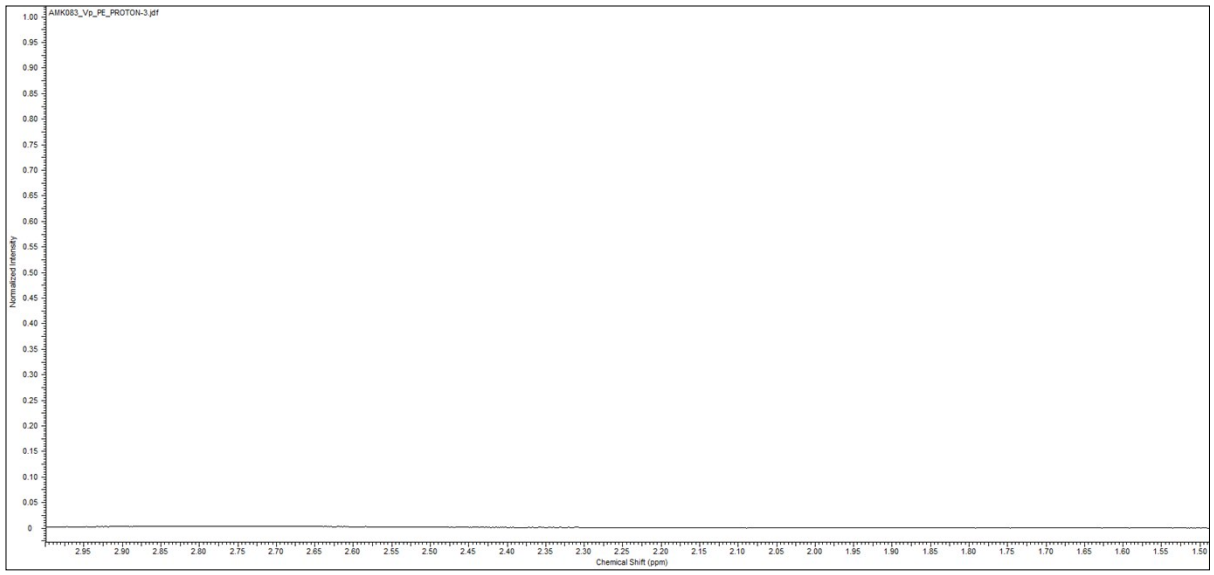

Figure S19: ^{1}H NMR spectrum of **SAMM-3-Cu-OTf**, post-exposure to PX/EB vapour. Magnified region: 1.5 – 3.0 ppm.

(b) Liquid-phase selectivity

Liquid-phase selectivity experiments were carried out by placing 30 mg of the crystalline powder of **SAMM-3-Cu-OTf** in a vial and adding 2 mL of an equimolar binary mixture of any of the C_8 isomers. The vials were allowed to stand at rt. After 72 h, the powder had partially crystallised into small crystals, which were filtered and placed in the fumehood for 30 mins. After drying, the crystals were dissolved in 1.5 mL of $CDCl_3$ and the solution was pipetted into NMR tubes for ^{1}H NMR analysis. Like the vapour phase experiment, the final liquid-phase selectivity value is an average obtained from three separate experiments, which were performed under identical conditions. Once again, the values for MX/PX, MX/EB and PX/EB were omitted, as there were no intensity peaks corresponding to these isomers on the NMR spectrum when OX was not present.

Batch no.	OX/MX	OX/PX	OX/EB
1	5.00	12.32	10.67
2	4.95	12.33	10.20
3	4.91	12.33	10.54
Average	4.95	12.33	10.47

Table S2: Selectivity values of **SAMM-3-Cu-OTf** for OX-containing isomer mixtures in the liquid phase.

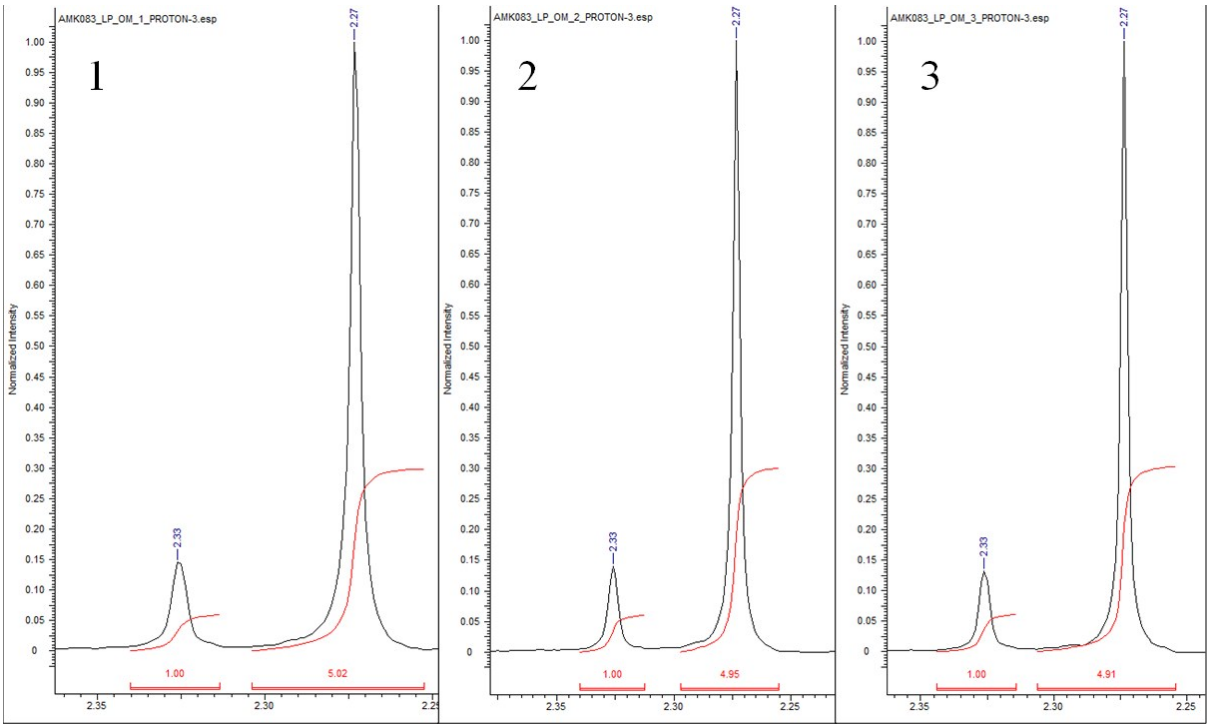

Figure S20: Magnified ^{1}H NMR spectrum for the methyl groups of MX (δ = 2.33) and OX (δ = 2.27) in a sample of **SAMM-3-Cu-OTf** soaked in an equimolar OX/MX mixture.

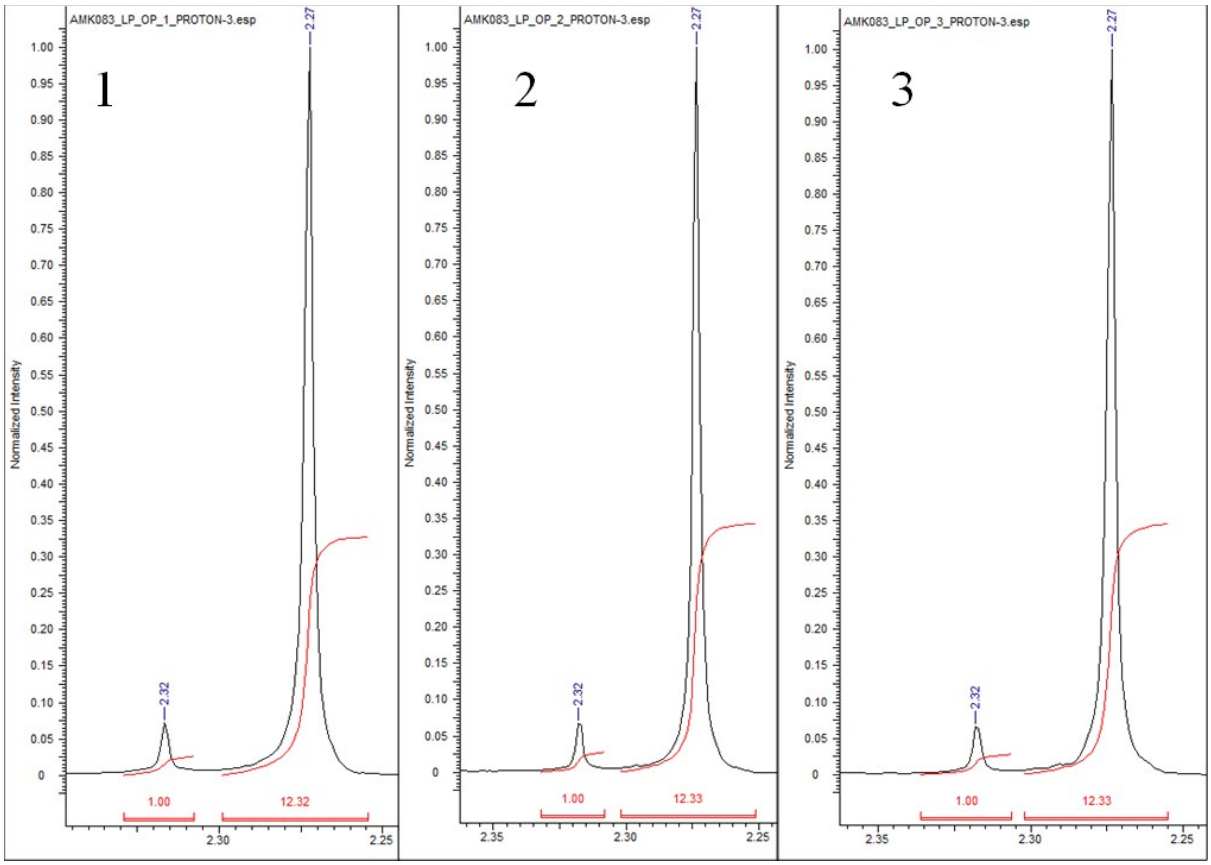

Figure S21: Magnified ^{1}H NMR spectrum for the methyl groups of PX (δ = 2.32) and OX (δ = 2.27) in a sample of **SAMM-3-Cu-OTf** soaked in an equimolar OX/PX mixture.

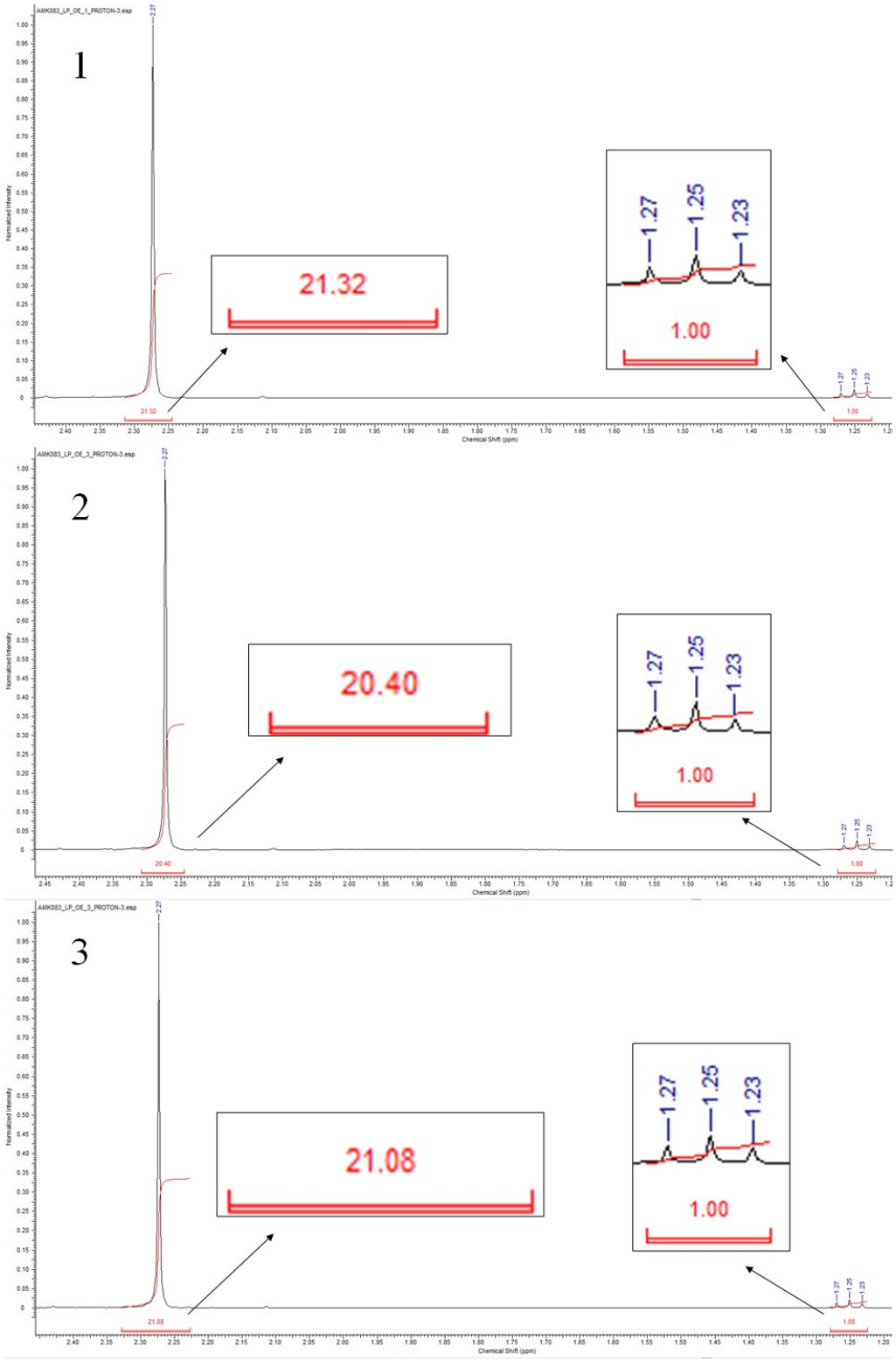

Figure S22: Magnified ^{1}H NMR spectrum for the methyl groups of EB (triplet) and OX (singlet) in a sample of **SAMM-3-Cu-OTf** soaked in an equimolar OX/EB mixture. The methyl group signal for OX represents twice as many protons as EB.

10. Intermolecular interactions

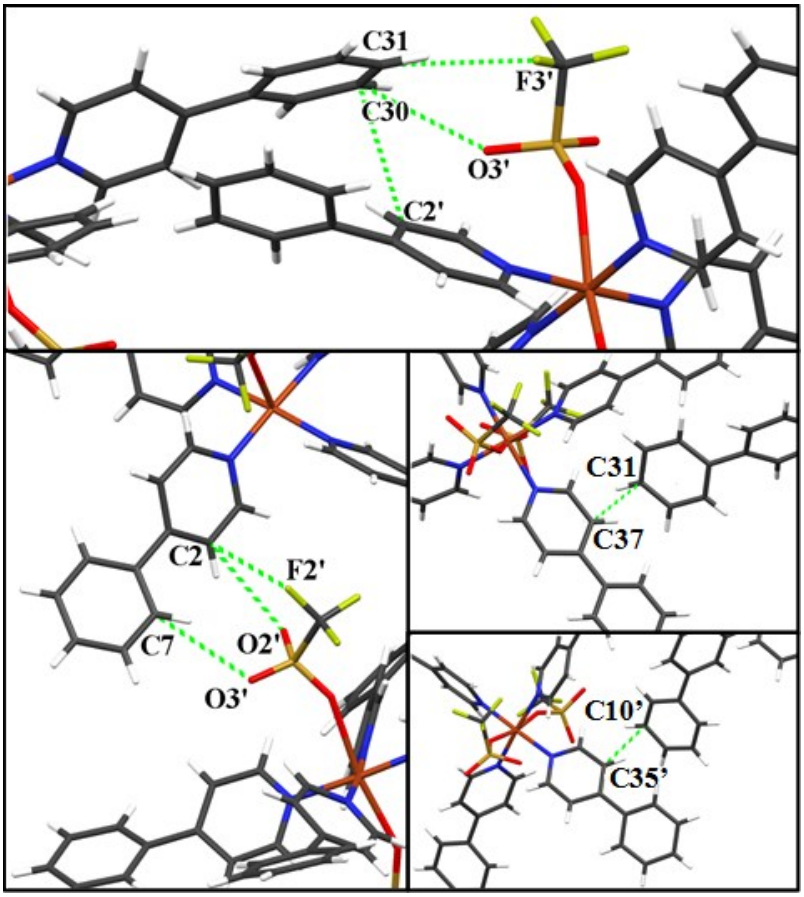

Figure S23: Host-host interactions in the α–phase. Colour code: same as in manuscript.

Type of interaction	Atoms	Distance (Å)
C-F ···π	F2' – C2	3.170 (9)
H-bond (C-H···O)	C2 – O2'	3.346(8)
	C7 – O3'	3.322(10)
	C30 – O3'	3.528(11)
H-bond (C-H ···F)	C31 – F3'	3.395(11)
C-H ···π	C2' – C30	3.530(9)

	C10’ – C35’	3.496(8)
π - π	C37 – C31	3.370(10)

Table S3: List of interactions governing the closed (α–) phase **SAMM-3-Cu-OTf**.

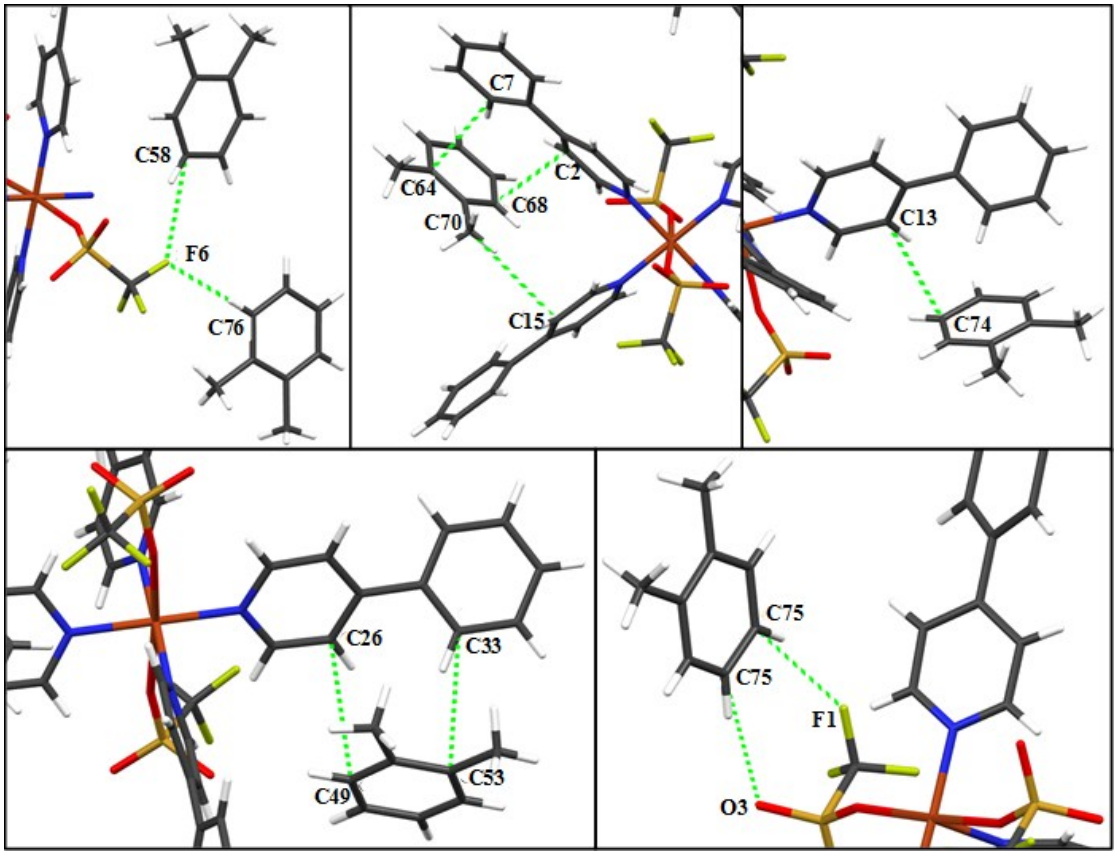

Figure S24: Host-guest interactions, which play key roles in the open phase **SAMM-3-Cu-OTf·4OX.**

Type of interaction	**Atoms**	**Distance (Å)**
H-bond (C-H ···F)	C58 – F6	3.35483(7)
	C76 – F6	3.53920(6)
	C75 – F1	3.35871(7)
H-bond (C-H ···O)	C74 – O3	3.54140(7)
π - π	C26 – C49	3.39744(6)
C-H ···π	C33 – C53	3.47336(6)

	C7 – C64	3.55826(6)
	C2 – C68	3.45226(6)
	C70 – C15	3.81701(8)
	C13 – C74	3.66190(12)

Table S4: List of interactions observed in **SAMM-3-Cu-OTf·4OX**.

11. Sorbents in Figures 3d-f

Number on graph	Material
1	CAU-13
2	CPO-27-Ni
3	$Zn(BDC)(Dabco)_{0.5}$
4	HKUST-1
5	MIL-47 (V)
6	$Co_2(dobdc)$
7	MIL-53 (Fe)
8	UiO-66
9	MIL-53 (Al)
10	sql-1-Co-NCS
11	$Ni(NCS)_2(ppp)_4$
12	MOF-5
13	MIL-53 (Ga)
14	MIL-53 (Cr)

Table S5: List of sorbents sorted by their corresponding numbers on the three graphs composing Figure 3 in the manuscript.

Material	OX Uptake (*wt %*)	OX/MX Selectivity	OX/PX Selectivity	OX/EB Selectivity	Network Type	Switching Sorbent (Y/N)
CAU-13[S7]	17.0	1.9	1.5	-	3D	N
CPO-27-Ni[S8]	20.1	1.7	3.3	-	3D	N
Zn(BDC)(Dabco)$_{0.5}$[S9]	25.0	1.1	1.9	1.6	3D	N
HKUST-1[S8]	29.7	1.1	1.2	-	3D	N
MIL-47(V) [S10,S11]	35.0	2	1.4	10.9	3D	N
Co$_2$(dobdc)[S12]	38.2	2.5	3.9	1.2	3D	Y
MIL-53(Fe)[S13]	39.0	1.6	2.53	-	3D	Y
UiO-66 [S14]	42.4	1.8	2.4	-	3D	N
MIL-53(Al)[S15-S17]	46.0	2.7	3.5	10.9	3D	Y
sql-1-Co-NCS[S18]	87.0	7.5	9.6	60.1	2D	Y
Ni(NCS)$_2$(ppp)$_4$[S19]	29.0	34.2	40.5	-	0D	Y
MOF-5[S20]	13.0	-	-	2.0	3D	N
MIL-53(Ga)[S17]	37.1	-	-	4.7	3D	Y
MIL-53(Cr)[S17]	42.4	-	-	4.9	3D	Y

Table S6: List of sorbents included in Figure 3(d-f) of the manuscript with their respective OX selectivities and saturation capacities in weight %.

***** Selectivity values for materials in tables S5 and S6 were reproduced from references S7-S20. In each case, the highest OX selectivity value reported for that material was chosen, regardless of whether the experiment was conducted with guest in liquid or vapour phase.

12. References

S1. APEX3. Ver. 2017.3-0. Bruker AXS Inc., Madison, Wisconsin, USA, **2017**.

S2. L. Krause, R. Herbst-Irmer, G. M. Sheldrick and D. Stalke, *J. Appl. Cryst.*, 2015, **48**, 3-10.

S3. XPREP Ver. 2014/2, Bruker AXS Inc., Madison, Wisconsin, USA, **2014**.

S4. G. Sheldrick, *Acta Cryst. A.*, 2015, **71**, 3-8.

S5. G. Sheldrick, *Acta Cryst. C.*, 2015, **71**, 3-8.

S6. O. V. Dolomanov, L. J. Bourhis, R. J. Gildea, J. A. K. Howard, H. Puschmann, *J. Appl. Cryst.*, 2009, **42**, 339-341.

S7. F. Niekiel, J. Lannoeye, H. Reinsch, A. S. Munn, A. Heerwig, I. Zizak, S. Kaskel, R. I. Walton, D. de Vos, P. Llewellyn, A. Lieb, G. Maurin, N. Stock, *Inorg. Chem.,* 2014, **53**, 4610-4620.

S8. D. Peralta, K. Barthelet, J. Pérez-Pellitero, C. Chizallet, G. Chaplais, A. Simon-Masseron, G. D. Pirngruber, *J. Phys. Chem. C,* 2012, **116**, 21844-21855.

S9. M. P. M. Nicolau, P. S. Bárcia, J. M. Gallegos, J. A. C. Silva, A. E. Rodrigues, B. Chen*, J. Phys. Chem. C*, 2009, **113**, 13173-13179.

S10. L. Alaerts, C. E. A. Kirshhock, M. Maes, M. A. van der Veen, V. Finsy, A. Depla, J. A. Martens, G. V. Baron, P. A. Jacobs, J. F. M. Denayer, D. E. De Vos, *Angew. Chem., Int. Ed*., 2007, **46**, 4293-4297.

S11. V. Finsy, H. Verelst, L. Alaerts, D. De Vos, P. A. Jacobs, G. V. Baron, J. F. M. Denayer, *J. Am. Chem.Soc*., 2008, **130**, 7110-7118.

S12. M. I. Gonzalez, M. T. Kapelewski, E. D. Bloch, P. J. Milner, D. A. Reed, M. R. Hudson, J. A. Mason, G. Barin, C. M. Brown, J. R. Long, *J. Am. Chem. Soc*. 2018, **140**, 3412-3422.

S13. R. El Osta, A. Carlin-Sinclair, N. Guillou, R. I. Walton, F. Vermoortele, M. Maes, D. de Vos, F. Millange, *Chem. Mater*., 2012, **24**, 2781-2791.

S14. M. A. Moreira, J. C. Santos, A. F. P. Ferreira, J. M. Loureiro, F. Ragon, P. Horcajada, K.-E. Shim, Y.-K. Hwang, U. H. Lee, J.-S. Chang, C. Serre, A. E. Rodrigues, *Langmuir,* 2012, **28**, 5715-5723.

S15. L. Alaerts, M. Maes, L. Giebeler, P. A. Jacobs, J. A. Martens, J. F. M. Denayer, C. E. A. Kirschhock, D. E. De Vos*, J. Am. Chem. Soc*., 2008, **130**, 14170-14178.

S16. V. Finsy, C. E. A. Kirschhock, G. Vedts, M. Maes, L. Alaerts, D. E. De Vos, G. V. Baron, J. F. M. Denayer, *Chem. – Eur. J*. 2009, **15**, 7724-7731.

S17. M. Agrawal, S. Bhattacharyya, Y. Huang, K. C. Jayachandrababu, C. R. Murdock, J. A. Bentley, A. Rivas-Cardona, M. M. Mertens, K. S. Walton, D. S. Sholl, S. Nair, *J. Phys. Chem. C*, 2018, **122**, 386-397.

S18. S-Q. Wang, S. Mukherjee, E. Patyk-Kazmierczak, S. Darwish, A. Bajpai, Q-Y. Yang, M. J. Zaworotko, *Angew. Chem. Int. Ed.,* 2019, **58**, 6630-6634.

S19. M. Lusi, L. J. Barbour, *Angew. Chem. Int. Ed*., 2012, **51**, 3928-3931.

S20. Z.-Y. Gu, D.-Q. Jiang, H.-F. Wang, X.-Y. Cui, X.-P. Yan, *J. Phys. Chem. C,* 2010, **114**, 311-316.